

Hyperspectral Image Super-Resolution with Spectral Mixup and Heterogeneous Datasets

Ke Li¹ Dengxin Dai¹ Ender Konukoglu¹ Luc Van Gool^{1,2}

¹CVL, ETH Zurich, ²PSI, KU Leuven

{ke.li, dai, ender.konukoglu, vangool}@vision.ee.ethz.ch

Abstract

This work studies Hyperspectral image (HSI) super-resolution (SR). HSI SR is characterized by high-dimensional data and a limited amount of training examples. This exacerbates the undesirable behaviors of neural networks such as memorization and sensitivity to out-of-distribution samples. This work addresses these issues with three contributions. First, we propose a simple, yet effective data augmentation routine, termed Spectral Mixup, to construct effective virtual training samples. Second, we observe that HSI SR and RGB image SR are correlated and develop a novel multi-tasking network to train them jointly so that the auxiliary task RGB image SR can provide additional supervision. Finally, we extend the network to a semi-supervised setting so that it can learn from datasets containing low-resolution HSIs only. With these contributions, our method is able to learn from heterogeneous datasets and lift the requirement for having a large amount of HD HSI training samples. Extensive experiments on four datasets show that our method outperforms existing methods significantly and underpin the relevance of our contributions. The code of this work will be released soon.

1. Introduction

Hyperspectral imaging acquires images across many intervals of the electromagnetic spectrum. It has been applied to numerous areas such as medical diagnosis [37], food quality and safety control [22], remote sensing [21] and object detection [39]. All these applications benefit from analyzing the spectral information coming with HSIs. One obstacle in the way of further unleashing this potential is data acquisition. Acquiring HSIs of high spatial and high spectral resolution at a high frame rate is still a grand challenge. There is still no camera to achieve these three goals at the same time. Cameras for a compromise setting – high spectral but low spatial resolution – are quite common by now, though still expensive. As a result, increasing efforts

have been made to advance HSI super-resolution (SR).

While numerous deep learning methods have been developed for improving the resolution of RGB images (RGBIs), the topic of HSI SR has received little attention. One of the main reasons is the lack of large-scale HSI datasets for high-resolution (HR) HSIs. As known, supervised deep learning methods need an enormous amount of training data. This situation, unfortunately, will not be improved in the foreseeable future due to the challenges hyperspectral imaging faces. In this work, we choose a different route and propose to learn from heterogeneous datasets and virtual examples. We find that while it is difficult to collect HR HSIs, it is relatively easy to collect only LR HSIs and it is very easy to collect HR RGB images. It is thus very appealing to have a HSI SR method which can learn from these heterogeneous sources. Our method is designed for this aim.

Although the data distribution is not the same between RGBIs and HSIs, the two SR tasks do share some common goals in integrating information from neighboring spatial regions and neighboring spectral bands during the learning. We embrace this observation and formulate both tasks into the same learning framework such that the parameter distribution induced by the RGBI SR task can serve as an effective regularization for our HSI SR task. The challenge lies in the difference in spectral band numbers, e.g. three in RGBIs vs. e.g. 31 or 128 in HSIs. To tackle this and to reduce the computational complexity, we propose a universal group convolutional neural network that can accommodate different spectral groups. We also expand the number of bands of RGBIs via a linear spectral interpolation. This way, the size of the group for the network can be chosen freely.

Semi-supervised learning (SSL) exploits unlabeled data to reduce over-fitting to the limited amount of labeled data [16, 31, 45, 48, 24]. While good progress has been achieved, the strategies are mainly designed for image classification and object recognition. Their applicability to a low-level dense regression task such as HSI SR has yet to be verified. In this work, we again leverage the success of RGBI SR and propose a cross-model consistency that favors functions giving consistent outputs between super-resolved

RGBIs and super-resolved HSIs. Basically, we convert LR HSIs into LR RGB images and pass those through the RGBI SR network. In the meanwhile, we pass the LR HSIs through our HSI SR network to get the super-resolved HSIs and convert them to RGBIs with a standard camera response function. We enforce the consistency between the two versions of super-resolved RGBIs. This way, supervision is transferred from the better-trained RGB SR network to our HSI SR network via a second route.

We further propose a data augmentation routine, termed *Spectral Mixup*, to create effective ‘virtual’ training examples. Data augmentation is a strategy to create virtual samples by modifying the original samples. Data augmentation is known to increase the generalizability of learning methods. Common methods for classification tasks include reflections, rotations, cropping, and color jittering. They assume that examples obtained by those operations share the same class with the original example and that can hardly be applied to our regression task. The recent work *mixup* [57] creates virtual examples by using convex combinations of pairs of examples and their labels to favor functions which preserve simple linear behavior in-between training examples. Motivated by these, we propose *Spectral Mixup* for HSI SR to create virtual samples using convex combinations of spectral bands of the same image. *Spectral Mixup* favors functions that preserve simple linear behavior in-between spectral bands. We show in experiments that it outperforms *mixup* for our task.

To summarize, this work makes three contributions: 1) a multi-tasking HSI SR method to learn together with an auxiliary RGBI SR task; 2) A SSL method to learn also from ‘unlabeled’ LR HSIs; and 3) a simple, yet effective data augmentation method *Spectral Mixup*.

2. Related Work

Hyperspectral Image Super-Resolution. HSI SR can be grouped into three categories according to their settings: 1) HSI SR from only RGBIs; 2) Single HSI SR from LR HSIs; and 3) HSI SR from both HR RGBIs and LR HSIs of the same scene. Our method belongs to the second group.

HSR SR from only RGBIs is a highly ill-posed problem. However, it has gained great traction in recent years due to its simple setup and the well-organized workshop challenges [8]. Similar to other computer vision topics, the trend has shifted from ‘conventional’ methods such as radial basis functions [40] and sparse coding [7] to deep neural networks [20, 44, 8]. This trend highlights the need for bigger training datasets.

Single image SR aims to model the relationship between the LR images and HR ones by learning from a collection of examples consisting of pairs of HR images and LR images. Single RGBI SR has achieved remarkable results in the last years. Since the first work of using neural networks for

the task [18], progress has been made in making networks deeper and the connections denser [27, 59], using feature pyramids [30], employing GAN losses [33], and modeling real-world degradation effects [23]. As to single HSI SR, there has been great early work [3, 60] as well. However, that is also surpassed by deep learning methods. For instance, Yuan *et al.* [54] trained a single-band SR method on natural image datasets, and applied it to HSIs in a band-wise manner to explore spatial information. The spectral information is explored via matrix factorization afterwards. In order to explore both spatial and spectral correlation at the same time, methods based on 3D Convolutional Networks [38, 34] have been developed. Although 3D CNNs sound like a perfect solution, the computational complexity is very high. To alleviate this, Grouped Convolutions (GCs) with shared parameters have been recently used in [35, 26]. While the backbone network of our method is also based on GCs, our three proposed contributions are all new.

Fusion-based methods use HR RGBIs of the same scene as references to improve the spatial resolution of the LR HSIs [12, 51]. This stream of methods have received more research attention than the former two. Many learning techniques have been applied to this data fusion task including Bayesian inference [5, 6, 58], matrix factorization [32, 17], sparse representation [4, 19], and deep neural networks [41, 49]. The common goal of these methods is to learn to propagate the detailed information in the HR RGBIs to the target HSIs and fuse them with the fundamental spectral information from LR HSIs. Despite the plethora of fusion algorithms developed, they all assume that the LR HSIs and the HR RGBIs are very well co-registered [26]. This data registration is a challenge on its own and registration errors will lead to degraded SR results [14, 61].

Learning with Auxiliary Tasks. It is quite a common practice to borrow additional supervision from related auxiliary tasks, when there is insufficient data to learn a task. The common strategy is to learn all the tasks together so that the auxiliary tasks can regularize the optimization. There are normally two assumptions: (1) we only care about the performance of the main task and (2) the supervision for the auxiliary tasks is easier to obtain than that of the main task. Previous work has employed various kinds of self-supervised methods as auxiliary tasks for the main supervised task in a semi-supervised setting [29, 11, 42]. For instance, generative approaches have been explored in [29] and predicting the orientation of image patches is used in [11]. Another related setting is multi-task learning (MTL) [46]. In MTL, the goal is to reach high performance on multiple tasks simultaneously, so all tasks are main tasks and all tasks are auxiliary tasks. While the goal is different, many strategies in MTL such as parameter sharing [10], task consistency [56], and loss balance [15] are useful for learning with auxiliary tasks.

3. Approach

HSIs provide tens of narrow bands, so processing all the bands together is time-consuming and requires very large datasets in order to avoid over-fitting. In this work, we follow [26] and use a grouping strategy to divide input HSIs into overlapping groups of bands. This way, the spectral correlation among neighboring bands can be effectively exploited without increasing the parameters of the model. Another major advantage of using a grouping strategy is that it offers the possibility to train our auxiliary task RGBI SR along with our main task HSI SR within the same network. Without using the grouping strategy, the difference in the number of bands is very large between the two tasks. In this work, we assume that the relationships between low/high-resolution HSIs and low/high-resolution RGBIs are correlated, so they should be trained together so that RGBI SR can provide additional supervision for HSI SR. This way, the HSI SR method can enjoy training samples of a much more diverse set of scenes especially those that cannot be captured well by current hyperspectral imaging devices such as moving objects.

3.1. HSI SR with an Auxiliary RGBI SR Task

Given two SR tasks \mathcal{T}_{HS} and \mathcal{T}_{RGB} , we aim to help improve the learning of a model for \mathcal{T}_{HS} by using the knowledge contained in \mathcal{T}_{RGB} . In the supervised setting, each task is accompanied by a training dataset consisting of N training samples, i.e., $\mathcal{D}_{\text{HS}} = \{\mathbf{x}_{\text{HS}}^i, \mathbf{X}_{\text{HS}}^i\}_{i=1}^{N_{\text{HS}}}$ and $\mathcal{D}_{\text{RGB}} = \{\mathbf{x}_{\text{RGB}}^i, \mathbf{X}_{\text{RGB}}^i\}_{i=1}^{N_{\text{RGB}}}$, where $\mathbf{x}_{\text{HS}} \in \mathbb{R}^{h_1 \times w_1 \times C}$, $\mathbf{X}_{\text{HS}} \in \mathbb{R}^{H_1 \times W_1 \times C}$, $\mathbf{x}_{\text{RGB}} \in \mathbb{R}^{h_2 \times w_2 \times Z}$, and $\mathbf{X}_{\text{RGB}} \in \mathbb{R}^{H_2 \times W_2 \times Z}$. We denote low-resolution (LR) images by \mathbf{x} , high-resolution (HR) images by \mathbf{X} , the number of bands of HSIs by C , the number of bands in RGB images by Z (3 here), and the size of the images by h, w, H and W . Given a scaling factor τ , we have $H_i = \tau h_i$ and $W_i = \tau w_i$ for both tasks.

The goal is to train a neural network Φ_{HS} to predict the HR HSI for a given LR HSI: $\mathbf{X}_{\text{HS}} = \Phi_{\text{HS}}(\mathbf{x}_{\text{HS}})$. Different from previous methods, which have a single network for the whole task, our method consists of three blocks: an encoder which is shared by the two SR tasks, and two task-specific decoders to output the final outputs. More specifically, $\Phi_{\text{HS}} = (\Phi^{\text{En}}, \Phi_{\text{HS}}^{\text{De}})$ and $\Phi_{\text{RGB}} = (\Phi^{\text{En}}, \Phi_{\text{RGB}}^{\text{De}})$. The general architecture is shown in Fig 1.

In order to share the same encoder between the two SR tasks, we divide the C input channels of \mathbf{x}_{HS} into groups of M bands. For HSI SR, the encoder network Φ^{En} takes M channels as input and generates M channels as output. The outputs of all the groups of \mathbf{x}_{HS} are then concatenated according to their original spectral band position to assemble a new HSI $\tilde{\mathbf{X}}_{\text{HS}} \in \mathbb{R}^{H_1 \times W_1 \times C}$. The neighboring groups of \mathbf{x}_{HS} can have overlaps and we average the results of the

overlapping areas when assembling $\tilde{\mathbf{X}}_{\text{HS}}$. There are two up-sampling layers to upscale the size of the input to the desired size in a progressive manner. This progressive upsampling has proven useful for both RGBI SR [30] and HSI SR [26]. The reconstructed $\tilde{\mathbf{X}}_{\text{HS}}$ is then fed into the decoder network $\Phi_{\text{HS}}^{\text{De}}$ as a whole to generate the final output $\hat{\mathbf{X}}_{\text{HS}}$, which is then compared to the ground truth \mathbf{X}_{HS} to compute the loss. $\Phi_{\text{HS}}^{\text{De}}$ takes all the bands directly to learn long-range spectral correlations beyond individual groups to refine the results.

For RGBI SR, we first increase the number of bands of \mathbf{x}_{RGB} from Z to M via a simple spectral interpolation which will be explained in Sec. 3.1.1. The interpolated M -band image is then passed through the encoder Φ^{En} to obtain a new M -band RGB image $\tilde{\mathbf{X}}_{\text{RGB}} \in \mathbb{R}^{H_2 \times W_2 \times M}$ of the desired resolution. Because the decoder is shared by two tasks, $\tilde{\mathbf{X}}_{\text{RGB}}$ is also needed to be fed to its own task-specific decoder network $\Phi_{\text{RGB}}^{\text{De}}$ for further refinement. The final output $\hat{\mathbf{X}}_{\text{RGB}}$ from $\Phi_{\text{RGB}}^{\text{De}}$ is then compared to the ground-truth image \mathbf{X}_{RGB} .

In order to have a modular design, the three sub-networks have the same basic architecture. They are all composed of a sequence of Spatial-Spectral Block (SSB) modules. The SBB module was proposed in [26] as a basic building block for their HSI SR network. Each SBB has a Spatial Residual Module and a Spectral Attention Residual Module. Two Convolutional layers (the first one followed by a ReLU layer) with 3x3 filters are used in the Spatial Residual Module to capture spatial correlations. Two Convolutional layers (the first one again followed by a ReLU layer) with 1x1 filters are used in the Spectral Attention Residual Module to capture spectral correlations. Please refer to the Fig.2 in [26] for more details of the SBB module. We construct the whole network with standard Convolutional Layers, SBBs, Upsampling Layers and Concatenation Operations. There are also skip connections at multiple scales to facilitate the information flow. The input LR images are also scaled to the desired size via Bicubic Interpolation and fused with the network output for residual learning. The complete network is shown in Fig. 1. We employ the PixelShuffle [43] operator for the upsampling layer. Given a scaling factor τ , the first upsampling layer upscales the features $\tau/2$ times and the second one handles the remaining $\times 2$ factor. The internal features of all SBB modules are limited to 256 in this work. The filter size of all Convolutional Layers, except for those in the Spectral Attention Residual Module of SBBs, are set to 3×3 .

3.1.1 Spectral Interpolation of RGB Images

The task is to increase the number of band from Z to M for RGB images. $Z = 3$ in this case and $M = 8$ in this work. Because the generated M -band images will be used to train the SR network for supervision transfer to HSI SR, we posit

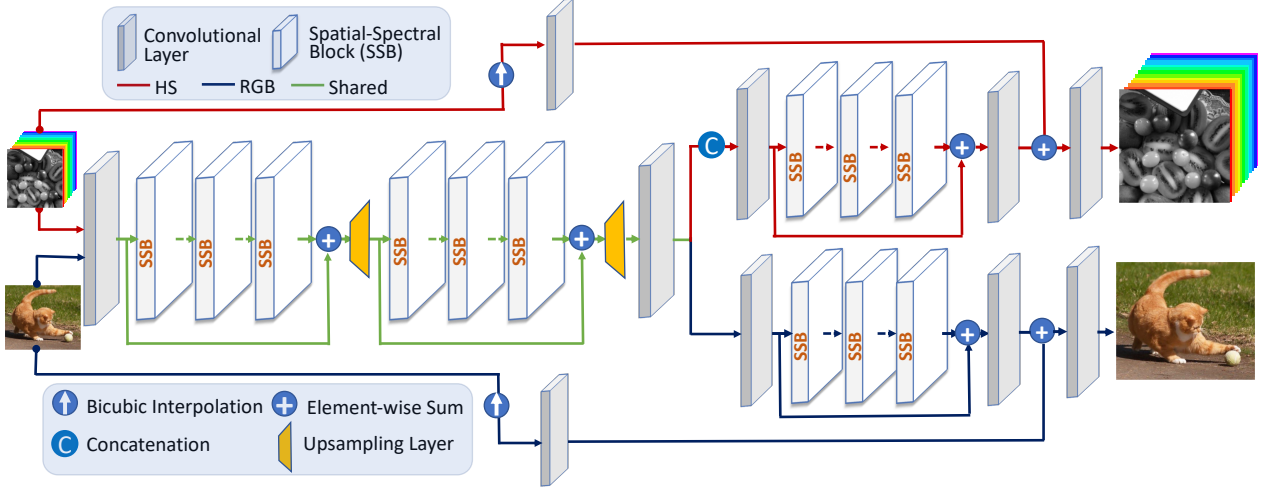


Figure 1: The architecture of our network consisting of a shared encoder and two specific decoders for the two SR tasks.

that these new images need to have certain properties. First, they should not contain artifacts. Second, the correlation between the bands of the new images should follow a distance rule in that the correlation between neighboring HSI bands should be higher than that between distant bands. For this, we propose a simple interpolation method. Given Z bands, we interpolate $K = (M - Z)/(Z - 1)$ new bands to each of the $Z - 1$ intervals between consecutive bands. For the i^{th} band $\hat{x}(i)$ between the original bands z and $z + 1$, we have:

$$\hat{x}(i) = (1 - \frac{i}{K+1})x(z) + \frac{i}{K+1}x(z+1). \quad (1)$$

Note that if K is not an integer, we use $\lceil K \rceil$ for the first interval and $\lfloor K \rfloor$ for the second one.

3.2. Spectral Mixup

Data augmentation is a strategy to create virtual samples by alternating the original samples. The recent *mixup* method [57] creates virtual examples by using convex combinations of pairs of examples and their labels. While it is very effective for high-level classification tasks, it does not offer help for low-level SR tasks [53] because the detailed image structures are broken up by their mixing up of two images. These detailed structures are important for SR tasks. Taking account of this observation, we propose a data augmentation routine *Spectral Mixup* specifically for HSI SR. It creates virtual samples and their ground truths by using convex combinations of spectral bands within self-image and within its ground-truth image, respectively.

More specifically, given \mathbf{x}_{HS} and its ground truth \mathbf{X}_{HS} , both with C channels, we generate a mixing matrix $B \in \mathbb{R}^{C \times C}$ filled with random numbers from a uniform distribution on the interval $[0, 1)$. B is then row-wise normalized

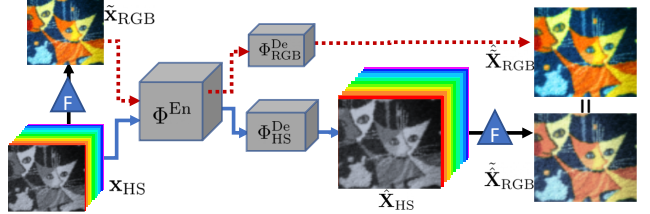


Figure 2: The pipeline of our semi-supervised learning.

to make sure that the values in the projected image have the same magnitude as that of the original image. The new example and its ground truth are then created as:

$$\hat{\mathbf{x}}_{\text{HS}}^{(i,j)} = \alpha \mathbf{x}_{\text{HS}}^{(i,j)} + (1 - \alpha) B \mathbf{x}_{\text{HS}}^{(i,j)}, \quad (2)$$

$$\hat{\mathbf{X}}_{\text{HS}}^{(i,j)} = \alpha \mathbf{X}_{\text{HS}}^{(i,j)} + (1 - \alpha) B \mathbf{X}_{\text{HS}}^{(i,j)}, \quad (3)$$

where (i,j) index over all positions to get the values of pixels. The randomly projected images are fused with the original images to strike a balance between increasing variations and preserving the fidelity of real HSIs. For instance, the relationships between the bands of real HSIs should be largely kept. In this work, α is set to 0.5 and we study the influence of this parameter in Sec. 4. The implementation of *Spectral Mixup* training is very straightforward and can be done with a few lines of code. *Spectral Mixup* also introduces very little computation overhead. By applying it, more examples from the vicinity of the original example can be sampled. Learning with those new examples encourages the network to have simple linear behavior in-between spectral bands which is found very useful for HSI SR.

3.3. Semi-Supervised HSI SR

While training with auxiliary RGB SR task and *Spectral Mixup* can greatly improve the performance, there is still a need to learn from unlabeled HSIs, *i.e.* LR HSIs without HR HSIs as ground truth. There are a diverse sets of methods developed for semi-supervised learning (SSL) such as entropy minimization and using pseudo-labels. However, they are mostly designed for high-level classification tasks and cannot be applied to HSI SR directly.

In this work, we propose a new SSL method specifically for HSI SR. For this purpose, we again leverage the fact that RGB SR is a better-addressed problem, given that it has a large amount of training data and it predicts only three channels. It works as follows: Given an image \mathbf{x}_{HS} , we convert it to an RGB image $\tilde{\mathbf{x}}_{\text{RGB}}$ with the response function of a standard RGB camera F : $\tilde{\mathbf{x}}_{\text{RGB}} = F(\mathbf{x}_{\text{HS}})$; The original HSI \mathbf{x}_{HS} and the converted RGB image $\tilde{\mathbf{x}}_{\text{RGB}}$ are then fed into the HSI SR network Φ_{HS} and the RGB SR network Φ_{RGB} , respectively, to generate the super-resolved results: $\hat{\mathbf{X}}_{\text{HS}} = \Phi_{\text{HS}}(\mathbf{x}_{\text{HS}})$ and $\hat{\mathbf{X}}_{\text{RGB}} = \Phi_{\text{RGB}}(\tilde{\mathbf{x}}_{\text{RGB}})$; $\hat{\mathbf{X}}_{\text{HS}}$ is then converted to an RGB image by using the same camera response function: $\tilde{\hat{\mathbf{X}}}_{\text{RGB}} = F(\hat{\mathbf{X}}_{\text{HS}})$. Finally, a consistency loss $L_{\text{ssl}}(\hat{\mathbf{X}}_{\text{RGB}}, \tilde{\hat{\mathbf{X}}}_{\text{RGB}})$ is computed between the two HR RGB results. This consistency check makes a good use of ‘unlabeled’ HSIs and ‘labeled’ RGB images. It transfers supervision from the RGB side to the HSI side. The diagram of this SSL method is shown in Fig. 2.

3.4. Loss Function

In order to capture both the spatial information and spectral correlation of the SR results, we follow [26] and combine the L1 loss and the spatial-spectral total variation (SSTV) loss [1]. SSTV is used to encourage smooth results in both spatial domain and spectral domain and it is defined as:

$$\mathcal{L}_{\text{SSTV}} = \frac{1}{N} \sum_{n=1}^N (||\nabla_{\text{h}} \hat{\mathbf{X}}^n||_1 + ||\nabla_{\text{w}} \hat{\mathbf{X}}^n||_1 + ||\nabla_{\text{c}} \hat{\mathbf{X}}^n||_1), \quad (4)$$

where ∇_{h} , ∇_{w} , and ∇_{c} compute gradient along the horizontal, vertical and spectral directions, respectively. The total loss is:

$$\mathcal{L} = \mathcal{L}_1 + \mathcal{L}_{\text{SSTV}}. \quad (5)$$

The overall loss for our SR tasks is:

$$\begin{aligned} \mathcal{L}_{\text{Total}} = & \mathcal{L}_{\text{HS}}(\mathbf{X}_{\text{HS}}, \hat{\mathbf{X}}_{\text{HS}}) + \mathcal{L}_{\text{SMixup}}(\hat{\mathbf{X}}_{\text{HS}}, \hat{\hat{\mathbf{X}}}_{\text{HS}}) \\ & + \mathcal{L}_{\text{RGB}}(\mathbf{X}_{\text{RGB}}, \hat{\mathbf{X}}_{\text{RGB}}) + \mathcal{L}_{\text{SSL}}(\hat{\mathbf{X}}_{\text{RGB}}, \tilde{\hat{\mathbf{X}}}_{\text{RGB}}). \end{aligned} \quad (6)$$

The main loss is augmented by the three auxiliary losses which are optional but highly beneficial. Since the final

loss combines multiple terms for leveraging heterogeneous datasets and virtual examples, it may introduce a few hyperparameters to balance the contributions of all terms. HSI SR methods with many hyperparameters can be problematic as the validation set is quite small normally to properly search for good values. However, we find in practice that the weights of those losses can be fixed to 1 and do not need to be tuned on a per-experiment or per-dataset basis. If desired, their contribution can be controlled by using different amount of training data for each loss and by altering the frequency of feeding training samples for each loss.

4. Experiments

4.1. Experimental Setup

Datasets. We evaluate our method on four public datasets. The datasets considered are three nature HSI datasets: CAVE dataset [50], Harvard dataset [13], and NTIRE 2020 dataset [8], and one remote sensing HSI dataset Chikusei [52]. Images in CAVE and NTIRE 2020 dataset have 31 bands ranging from 400 nm to 700 nm at a step of 10 nm. Images in Harvard dataset contain 31 bands as well but range from 420 nm to 720 nm. The Chikusei dataset has 128 bands spanning from 363 nm to 1018 nm.

The CAVE dataset contains 32 images of 512 x 512 pixels. We use 20 images for training and 10 images for testing. We evaluated in a supervised setting and a semi-supervised setting. For our semi-supervised setting, 1/4 of the training data is considered as the labeled set and the remaining 3/4 considered as unlabeled. For the Harvard dataset, there are 50 images in total. We use 40 for training and 10 for test. For the semi-supervised setting, 6 images are taken as the labeled images (with HR HSIs) while the remaining 34 are taken as unlabeled images. For NTIRE 2020, there are 480 images. We use 400 images for training and 80 images for test. For the semi-supervised case, we further split the 400 images into 100 as labeled images and 300 as unlabeled images. For Chikusei, there is only one big image of 2517 x 2335 pixels. We cropped 4 image crops of 256 x 256 pixels for test and use the rest for training. For the auxiliary RGB SR task, we adopt the DIV2K Dataset [2]. Because the resolution of DIV2K is much higher than our HSIs, we first downsample them by a factor of $\times 2$ and take these downsampled images as our HR RGB images.

Methods. We compare the proposed method to four state-of-the-art HSI SR methods: GDRRN [35], 3DFCNN [38], SSPSR [26], and MCNet [34]. We use exactly the same training data for all methods and use the default training settings given by the authors of these methods. Bicubic interpolation is also introduced as a baseline.

Training Details. The method is implemented with PyTorch. We use the ADAM optimizer [28] and train all variants of our method for 10 epoches. This is a small number

Methods	Components			CAVE			Harvard			NTIRE		
	RGBSR	<i>SMixup</i>	SSL	RMSE ↓	MPSNR ↑	ERGAS ↓	RMSE ↓	MPSNR ↑	ERGAS ↓	RMSE ↓	MPSNR ↑	ERGAS ↓
Ours				0.01282	41.38106	3.99731	0.01411	40.42362	3.20297	0.01675	37.76302	2.36922
Ours	✓			0.01191	42.01763	3.63288	0.01366	40.69577	3.11316	0.01583	38.21667	2.27241
Ours		✓		0.01246	42.08879	3.54516	0.01375	40.63699	3.12395	0.01542	38.56435	2.16249
Ours	✓	✓		0.01173	42.57401	3.40209	0.01348	40.80286	3.07281	0.01515	38.75436	2.11092
Ours	✓		✓	0.01187	42.21247	3.53264	0.01351	40.81661	3.06886	0.01547	38.55183	2.16476
Ours (final)	✓	✓	✓	0.01138	42.74453	3.31609	0.01335	40.89392	3.03947	0.01507	38.83877	2.09341
Bicubic	-	-	-	0.01856	38.73800	5.27190	0.01678	38.89758	3.80698	0.02353	34.74012	3.19014
GDRRN [35]	-	-	-	0.02048	37.59559	5.76242	0.01655	38.24997	4.72408	0.02484	33.94214	3.68688
3DFCNN [38]	-	-	-	0.01686	38.32237	8.81439	0.01578	39.30286	3.66444	0.02080	35.83412	2.82781
SSPSR [26]	-	-	-	0.01349	41.46318	3.91284	0.01422	40.34668	3.22915	0.01721	37.58708	2.37159
MCNet [34]	-	-	-	0.01362	41.28549	4.16636	0.01463	40.18194	3.27906	0.01613	38.45578	2.19636

Table 1: Results of all methods on the CAVE, Harvard, and NTIRE datasets in the semi-supervised setting for the $\times 4$ case. **Bold** indicates the best results. RGBSR means learning with auxiliary RGBI SR. *SMixup* is our *Spectral Mixup*.

Methods	Components			Metrics					
	RGBSR	<i>SMixup</i>	SSL	RMSE ↓	CC ↑	MPSNR ↑	MSSIM ↑	ERGAS ↓	SAM ↓
Ours				0.01230	0.94992	39.71319	0.93529	5.32514	2.58381
Ours	✓			0.01211	0.95161	39.86037	0.93691	5.22631	2.53569
Ours		✓		0.01216	0.95097	39.82008	0.93649	5.26244	2.56245
Ours	✓	✓		0.01215	0.95096	39.8338	0.93675	5.24407	2.59671
Ours	✓		✓	0.01219	0.95109	39.81107	0.93617	5.25279	2.56749
Ours (final)	✓	✓	✓	0.01181	0.95375	40.09431	0.94035	5.08513	2.49154

Table 2: Results of all methods on the Chikusei dataset in the semi-supervised setting for the $\times 4$ case. **Bold** indicates the best results. RGBSR means our auxiliary RGBI SR task. *SMixup* is our *Spectral Mixup*.

compared to the ones used by comparison methods. For instance, GDRRN [35] trains for 30 epoches, 3DFCNN [38] trains for 200 epoches, SSPSR [26] for 40 epoches, and MCNet [34] for 200 epoches. We choose a small number in order to thoroughly evaluate all the variants of our method. We find that 10 epoches are sufficient to give good results for our method, and believe a larger number probably can further push the numbers up. The initial learning rate of all our methods is set to 10^{-4} and is reduced by a factor of 0.3 after every 3 epoches. As to the batch size, 16 is used for all the methods. For our method, when the SSL loss is used, we use 8 due to the GPU memory limit.

Evaluation Metrics. We follow the literature [26] and evaluate the performance of all methods under six widely used metrics. They are cross correlation (CC) [36], spectral angle mapper (SAM) [55], root mean squared error (RMSE), erreur relative globale adimensionnelle de synthèse (ERGAS) [47], peak signal-to-noise ratio (PSNR), and structure similarity (SSIM) [62]. For PSNR and SSIM of the reconstructed HSIs, their mean values of all spectral bands are reported. CC, SAM, and ERGAS are widely used in HSI fusion task, while the other three are standard metrics for image restoration and RGBI SR. Due to space limit, for

some experiments, we only report numbers of three metrics and put the rest into the supplementary material.

Other Parameters. In this work, we focus on scaling factor $\times 4$ and $\times 8$. We report the results for $\times 4$ in the main paper, and report the results of $\times 8$ in the supplementary material. For the case of $\times 4$, we crop the images into patches of 64×64 pixels without overlapping to collect the training data. For $\times 8$, we use patches of 128×128 pixels. Those patches are then downsampled via Bicubic interpolation to obtain the corresponding LR HSI patches. We use group size 8, *i.e.*, $M = 2$, with an overlap of 2 by following [26]. The response function of Canon 1D Mark 3 [25] is used. In all the main experiments, the size of the RGB dataset is 3 times of the ‘labeled’ HSI dataset, so its size changes on a per-dataset basis. α is set to 0.5. The influence of some of these choices will be studied in Sec. 4.3.

4.2. Main Results

We first present the results in the semi-supervised setting. The results of all competing methods and all variants of our method on the CAVE, Harvard, and NTIRE dataset are shown in Table 1. The results in this table show that our method outperforms all other state-of-the-art methods

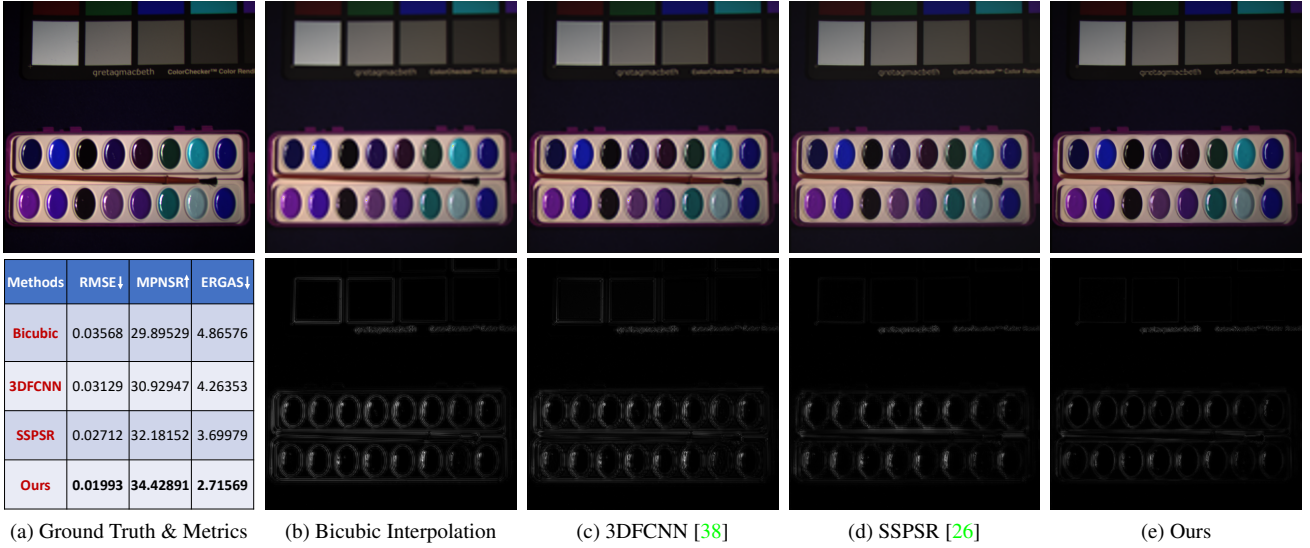


Figure 3: Exemplar results of our method and two competing methods trained in the semi-supervised setting on the CAVE dataset: top row for the super-resolved results and bottom row for the error maps.

Methods	Components		CAVE			Harvard		
	RGBSR	SMixup	RMSE ↓	MPSNR ↑	ERGAS ↓	RMSE ↓	MPSNR ↑	ERGAS ↓
Ours			0.01196	42.38359	3.45903	0.01344	40.91014	3.01039
Ours	✓		0.01109	42.73668	3.35884	0.01325	41.03709	2.96643
Ours		✓	0.01134	42.88402	3.28051	0.01317	41.08568	2.95718
Ours	✓	✓	0.01068	43.32421	3.11799	0.01321	41.05925	2.96496
GDRRN [35]	-	-	0.01629	39.74705	4.52683	0.01484	39.62759	3.67932
3DFCNN [38]	-	-	0.01583	39.21786	5.41798	0.01519	39.66271	3.47738
SSPSR [26]	-	-	0.01245	42.13787	3.55146	0.01352	40.81499	3.05007
MCNet [34]	-	-	0.01245	42.25978	3.56246	0.01405	40.59229	3.10529

Table 3: Results of all methods on the CAVE and Harvard datasets in the fully-supervised setting for the $\times 4$ case). **Bold** indicates the best results. RGBSR means our auxiliary RGBI SR task. SMixup is our *Spectral Mixup*.

significantly and consistently over all datasets and under all evaluation metrics. We would like to point out that our baseline model – our method without any of the three proposed contributions – is already a top-performing method and performs better than other comparing methods.

The good performance of our base model is mainly from its network design. Our deep group convolutional network is built on top of the recent work by Jiang *et al.* [26] with extensions. The major differences are: 1) we have used a deeper encoder (brunch) network, and 2) we have moved all the upsampling layers into the encoder and have removed a bottleneck layer (an intermediate image reconstruction layer with M channels) between the two upsampling layers. We find that these two changes improve the results. We also find that 3D convolution based methods are computationally heavy. That is probably the reason why the network

of [38] is quite shallow. We believe that this is the reason why their method does not give top results. When compared to the very recent method MCNet [34], our base model also performs better in almost all cases. This is especially interesting because MCNet is trained for 200 epoches while our method is trained only for 10 epoches. Our results reinforce the findings made in [26] that group convolutional networks are good at extracting the correlation between spectral bands without increasing the model size.

We can also find that our proposed contributions, namely training with the auxiliary task RGBI SR, data augmentation via *Spectral Mixup* and the semi-supervised learning method based on cross-model consistency, all contribute positively and significantly to the final results. It is worth noticing that these improvements are made on top of our strong base model. This means the improvements are not

Methods	RMSE ↓	MPSNR ↑	ERGAS ↓
Band Duplication	0.01222	41.91422	3.68148
Band Interpolation	0.01211	42.01642	3.58993

Table 4: Ablation study for RGB Band Interpolation.

Methods	RMSE ↓	MPSNR ↑	ERGAS ↓
Spatial Mixup [57]	0.01198	42.22387	3.52199
Cutblur Mixup [53]	0.01199	42.38385	3.44848
Spectral Mixup	0.01173	42.57401	3.40209

Table 5: Ablation study for *Spectral Mixup*

easy to achieve and are of great value. Out of the three, learning with the auxiliary task RGBI SR and *Spectral Mixup* can be used individually. The SSL component needs to be used together with the auxiliary task RGBI SR. As the results on all the datasets show, our SSL method can provide further improvement on top of the auxiliary RGBI SR method. We can also find from the tables that when the three components are combined together, we get the best performance – better than using any subsets of the proposed contributions. These observations are also well supported by our results on Chikusei with 128 bands in Table 2. We would like to point out that while the general philosophy of learning with auxiliary tasks is well known, the challenge and novelty often lie in defining proper auxiliary tasks for a new main task. Many seemingly-related auxiliary tasks yield no improvement or even degrade the performance of the main task [42].

When more supervision is given such as in the fully-supervised setting, all conclusions we drawn in the semi-supervised setting still hold. The results show that the proposed components are very effective and can be applied to situations with varying amount of HR HSIs. The superior performance of our method shows that it is able to learn from heterogeneous datasets and virtual examples rather than from purely HR HSIs. This greatly increases the amount of training data that can be used for HSI SR and can even learn with samples of scenes that cannot be captured easily with the current hyperspectral imaging devices such as moving objects. These improvements, however, comes at a cost of increased training time and the requirement for two additional datasets. However, large-scale RGB images are easily accessible and large-scale LR HSIs are also relatively easy to obtain, especially given the recent progress in single shot hyperspectral imaging [9].

We show visual results by our method and two competing methods in Fig. 3. The figure shows that our method yields the best results as well. More results can be found in the supplementary material.

4.3. Ablation Study

We analyze the choices made in our method here. All experiments are done with the CAVE dataset in the semi-supervised setting. Our first ablation study is on the size of the RGB dataset used for the RGBI SR. We found that for a small dataset such as CAVE, having a larger RGB dataset is beneficial. For instance, a dataset 6 times as large as the labeled CAVE dataset is better than 3 in the semi-supervised case. However, this advantage gets insignificant as the HSI dataset gets larger. We chose 3 for all our experiments for due to its faster training speed.

Second, we analyze the influence of α . We tested five values for it: 0, 0.25, 0.5, 0.75 and 1 and obtained the following RMSE results: 0.01175 0.01178, 0.01173, 0.01187, and 0.01189. We find α should not be too big or too small. We choose $\alpha = 0.5$ and use this in all our experiments to keep a good balance between increasing data variation and preserving the fidelity of real HSIs.

Third, we compare our band interpolation method (Eq. 1) to a simple band duplication method which generate the M bands as [BGRBGRBG] for our case. The results of these two methods are shown in Table 4. The table shows that our spectral interpolation method outperforms this simple duplication method. This interpolation method makes it possible to train HSI SR along with auxiliary RGBI SR. The interpolation is better than duplication because it preserves the general relationship between bands – neighboring bands have higher correlation than distant ones. The importance of having this method is that the value of M can be chosen freely instead of fixing to Z . The optimal value for M may not be Z in most of the cases.

Finally, we compare *Spectral Mixup* to two recent data augmentation methods *mixup* [57] and *CutblurMixup* [53]. These methods also rely on the data mixing idea. Note that the results for this experiment are generated under a joint training with the auxiliary RGBI SR module as this is a stronger method than our base model. The results in Table 5 show that *Spectral Mixup* outperforms both of the methods clearly. The spatial mixing method [57] blends data from two images. It may break detailed structures that are important for SR tasks. The *CutblurMixup* method learns *where to perform the SR* and is found helpful for RGB SR [53]. However, it does not work for our task. *Spectral Mixup* creates virtual examples by using convex combinations of spectral bands of the same image which avoids breaking image structures and preserves simple linear behavior in-between spectral bands. A combination of between-image mixup [57] and between-band mixup is interesting.

5. Conclusion

In this paper, we have proposed a new method for hyperspectral image (HSI) super-resolution (SR). We

build a deep group convolutional network which yields the state-of-the-art results. To further improve it, we have proposed three contributions. First, we extend the network such that the HSI SR task can be trained together with an auxiliary RGB image SR task to gain more supervision. Second, a simple, yet effective data augmentation method *Spectral Mixup* is proposed to create virtual training samples for HSI SR to increase the robustness of the network to new examples. Finally, the network is extended to also learn from datasets with LR HSIs only. The contributions greatly increase the amount of training data that HSI SR methods can use. Extensive experiments show that all the three contributions are important and they help our method set a new state of the art on four public datasets.

References

- [1] H. K. Aggarwal and A. Majumdar. Hyperspectral image denoising using spatio-spectral total variation. *IEEE Geoscience and Remote Sensing Letters*, 13(3):442–446, 2016. [5](#)
- [2] E. Agustsson and R. Timofte. Ntire 2017 challenge on single image super-resolution: Dataset and study. In *IEEE Conference on Computer Vision and Pattern Recognition Workshops (CVPRW)*, 2017. [5](#)
- [3] T. Akgun, Y. Altunbasak, and R. M. Mersereau. Super-resolution reconstruction of hyperspectral images. *IEEE Transactions on Image Processing*, 14(11):1860–1875, 2005. [2](#)
- [4] Naveed Akhtar, Faisal Shafait, and Ajmal Mian. Sparse spatio-spectral representation for hyperspectral image super-resolution. In *ECCV*, 2014. [2](#)
- [5] N. Akhtar, F. Shafait, and A. Mian. Bayesian sparse representation for hyperspectral image super resolution. In *CVPR*, 2015. [2](#)
- [6] Naveed Akhtar, Faisal Shafait, and Ajmal Mian. Hierarchical beta process with gaussian process prior for hyperspectral image super resolution. In Bastian Leibe, Jiri Matas, Nicu Sebe, and Max Welling, editors, *ECCV*, 2016. [2](#)
- [7] Boaz Arad and Ohad Ben-Shahar. Sparse recovery of hyperspectral signal from natural rgb images. In *ECCV*, 2016. [2](#)
- [8] Boaz Arad, Radu Timofte, Ohad Ben-Shahar, Yi-Tun Lin, and Graham D. Finlayson. Ntire 2020 challenge on spectral reconstruction from an rgb image. In *Proceedings of the IEEE/CVF Conference on Computer Vision and Pattern Recognition (CVPR) Workshops*, June 2020. [2](#), [5](#)
- [9] Seung-Hwan Baek, Incheol Kim, Diego Gutierrez, and Min H. Kim. Compact single-shot hyperspectral imaging using a prism. *ACM Transactions on Graphics (Proc. SIGGRAPH Asia 2017)*, 36(6):217:1–12, 2017. [8](#)
- [10] Arun Balajee Vasudevan, Dengxin Dai, and Luc Van Gool. Semantic object prediction and spatial sound prediction with binaural sounds. In *European Conference on Computer Vision (ECCV)*, 2020. [2](#)
- [11] Lucas Beyer, Xiaohua Zhai, Avital Oliver, and Alexander Kolesnikov. S4L: self-supervised semi-supervised learning. In *ICCV*, 2019. [2](#)
- [12] J. M. Bioucas-Dias, A. Plaza, N. Dobigeon, M. Parente, Q. Du, P. Gader, and J. Chanussot. Hyperspectral unmixing overview: Geometrical, statistical, and sparse regression-based approaches. *IEEE Journal of Selected Topics in Applied Earth Observations and Remote Sensing*, 5(2):354–379, 2012. [2](#)
- [13] A. Chakrabarti and T. Zickler. Statistics of Real-World Hyperspectral Images. In *CVPR*, 2011. [5](#)
- [14] C. Chen, Y. Li, W. Liu, and J. Huang. Sirf: Simultaneous satellite image registration and fusion in a unified framework. *IEEE Transactions on Image Processing*, 24(11):4213–4224, 2015. [2](#)
- [15] R. Cipolla, Y. Gal, and A. Kendall. Multi-task learning using uncertainty to weigh losses for scene geometry and semantics. In *CVPR*, 2018. [2](#)
- [16] Dengxin Dai and Luc Van Gool. Ensemble projection for semi-supervised image classification. In *ICCV*, 2013. [1](#)
- [17] R. Dian, L. Fang, and S. Li. Hyperspectral image super-resolution via non-local sparse tensor factorization. In *CVPR*, pages 3862–3871, 2017. [2](#)
- [18] C. Dong, C. C. Loy, K. He, and X. Tang. Image super-resolution using deep convolutional networks. *IEEE Transactions on Pattern Analysis and Machine Intelligence*, 38(2):295–307, 2016. [2](#)
- [19] W. Dong, F. Fu, G. Shi, X. Cao, J. Wu, G. Li, and X. Li. Hyperspectral image super-resolution via non-negative structured sparse representation. *IEEE Transactions on Image Processing*, 25(5):2337–2352, 2016. [2](#)
- [20] S. Galliani, Charis Lanaras, D. Marmanis, E. Baltsavias, and K. Schindler. Learned spectral super-resolution. *ArXiv*, abs/1703.09470, 2017. [2](#)
- [21] Alexander F.H. Goetz. Three decades of hyperspectral remote sensing of the earth: A personal view. *Remote Sensing of Environment*, 113:S5 – S16, 2009. [1](#)
- [22] A.A. Gowen, C.P. O’Donnell, P.J. Cullen, G. Downey, and J.M. Frias. Hyperspectral imaging – an emerging process analytical tool for food quality and safety control. *Trends in Food Science & Technology*, 18(12):590 – 598, 2007. [1](#)
- [23] Yong Guo, Jian Chen, Jingdong Wang, Qi Chen, Jiezhong Cao, Zeshuai Deng, Yanwu Xu, and Minghui Tan. Closed-loop matters: Dual regression networks for single image super-resolution. In *CVPR*, 2020. [2](#)
- [24] Lukas Hoyer, Dengxin Dai, Yuhua Chen, Adrian Köring, Suman Saha, and Luc Van Gool. Three ways to improve semantic segmentation with self-supervised depth estimation. *arXiv preprint arXiv:2012.10782*, 2020. [1](#)
- [25] J. Jiang, D. Liu, J. Gu, and S. Süsstrunk. What is the space of spectral sensitivity functions for digital color cameras? In *2013 IEEE Workshop on Applications of Computer Vision (WACV)*, 2013. [6](#)
- [26] J. Jiang, H. Sun, X. Liu, and J. Ma. Learning spatial-spectral prior for super-resolution of hyperspectral imagery. *IEEE Transactions on Computational Imaging*, 6:1082–1096, 2020. [2](#), [3](#), [5](#), [6](#), [7](#), [12](#), [13](#), [14](#), [15](#), [16](#)

- [27] J. Kim, J. K. Lee, and K. M. Lee. Accurate image super-resolution using very deep convolutional networks. In *CVPR*, 2016. 2
- [28] Diederik P. Kingma and Jimmy Ba. Adam: A method for stochastic optimization. In *ICLR*, 2015. 5
- [29] Durk P Kingma, Shakir Mohamed, Danilo Jimenez Rezende, and Max Welling. Semi-supervised learning with deep generative models. In *NeurIPS*. 2014. 2
- [30] W. Lai, J. Huang, N. Ahuja, and M. Yang. Deep laplacian pyramid networks for fast and accurate super-resolution. In *CVPR*, 2017. 2, 3
- [31] Samuli Laine and Timo Aila. Temporal ensembling for semi-supervised learning. In *ICLR*, 2017. 1
- [32] C. Lanaras, E. Baltsavias, and K. Schindler. Hyperspectral super-resolution by coupled spectral unmixing. In *2015 IEEE International Conference on Computer Vision (ICCV)*, 2015. 2
- [33] Christian Ledig, Lucas Theis, Ferenc Huszar, Jose Caballero, Andrew Cunningham, Alejandro Acosta, Andrew Aitken, Alykhan Tejani, Johannes Totz, Zehan Wang, and Wenzhe Shi. Photo-realistic single image super-resolution using a generative adversarial network. In *CVPR*, 2017. 2
- [34] Qiang Li, Qi Wang, and Xuelong Li. Mixed 2d/3d convolutional network for hyperspectral image super-resolution. *Remote Sensing*, 12(10), 2020. 2, 5, 6, 7, 12, 13, 14, 15, 16
- [35] Y. Li, Lei Zhang, C. Ding, Wei Wei, and Y. Zhang. Single hyperspectral image super-resolution with grouped deep recursive residual network. *2018 IEEE Fourth International Conference on Multimedia Big Data (BigMM)*, 2018. 2, 5, 6, 7, 12, 13, 14, 15, 16
- [36] L. Loncan, L. B. de Almeida, J. M. Bioucas-Dias, X. Briottet, J. Chanussot, N. Dobigeon, S. Fabre, W. Liao, G. A. Licciardi, M. Simões, J. Tournet, M. A. Veganzones, G. Vivone, Q. Wei, and N. Yokoya. Hyperspectral pansharpening: A review. *IEEE Geoscience and Remote Sensing Magazine*, 3(3):27–46, 2015. 6
- [37] Guolan Lua and Baowei Fei. Medical hyperspectral imaging: a review. *Journal of Biomedical Optics*, 2014. 1
- [38] Shaohui Mei, Xin Yuan, Jingyu Ji, Yifan Zhang, Shuai Wan, and Qian Du. Hyperspectral image spatial super-resolution via 3d full convolutional neural network. *Remote Sensing*, 9(11), 2017. 2, 5, 6, 7, 12, 13, 14, 15, 16
- [39] N. M. Nasrabadi. Hyperspectral target detection : An overview of current and future challenges. *IEEE Signal Processing Magazine*, 31(1):34–44, 2014. 1
- [40] Rang M. H. Nguyen, Dilip K. Prasad, and Michael S. Brown. Training-based spectral reconstruction from a single rgb image. In *ECCV*, 2014. 2
- [41] Ying Qu, Hairong Qi, and Chiman Kwan. Unsupervised sparse dirichlet-net for hyperspectral image super-resolution. In *CVPR*, 2018. 2
- [42] Baifeng Shi, Judy Hoffman, Kate Saenko, Trevor Darrell, and Huijuan Xu. Auxiliary task reweighting for minimum-data learning. In *NeurIPS*, 2020. 2, 8
- [43] W. Shi, J. Caballero, F. Huszár, J. Totz, A. P. Aitken, R. Bishop, D. Rueckert, and Z. Wang. Real-time single image and video super-resolution using an efficient sub-pixel convolutional neural network. In *CVPR*, 2016. 3
- [44] Z. Shi, C. Chen, Z. Xiong, D. Liu, and F. Wu. Hscnn+: Advanced cnn-based hyperspectral recovery from rgb images. In *IEEE/CVF Conference on Computer Vision and Pattern Recognition Workshops (CVPRW)*, 2018. 2
- [45] Antti Tarvainen and Harri Valpola. Mean teachers are better role models: Weight-averaged consistency targets improve semi-supervised deep learning results. 2017. 1
- [46] Simon Vandenhende, Stamatios Georgoulis, Marc Proesmans, Dengxin Dai, , and Luc Van Gool. Multi-task learning for dense prediction tasks: A survey, 2020. 2
- [47] L. Wald. Data fusion: definitions and architectures: fusion of images of different spatial resolutions. In *Presses des MINES*, 2002. 6
- [48] Qizhe Xie, Minh-Thang Luong, Eduard Hovy, and Quoc V. Le. Self-training with noisy student improves imagenet classification. In *CVPR*, 2020. 1
- [49] Qi Xie, Minghao Zhou, Qian Zhao, Deyu Meng, Wangmeng Zuo, and Zongben Xu. Multispectral and hyperspectral image fusion by MS/HS fusion net. In *CVPR*, 2019. 2
- [50] F. Yasuma, T. Mitsunaga, D. Iso, and S. K. Nayar. Generalized assorted pixel camera: Postcapture control of resolution, dynamic range, and spectrum. *IEEE Transactions on Image Processing*, 19(9):2241–2253, 2010. 5
- [51] N. Yokoya, C. Grohnfeldt, and J. Chanussot. Hyperspectral and multispectral data fusion: A comparative review of the recent literature. *IEEE Geoscience and Remote Sensing Magazine*, 5(2):29–56, 2017. 2
- [52] N. Yokoya and A. Iwasaki. Airborne hyperspectral data over chikusei. *Space Application Laboratory, University of Tokyo, Japan, Tech. Rep. SAL-2016-05-27*, May 2016. 5
- [53] Jaejun Yoo, Namhyuk Ahn, and Kyung-Ah Sohn. Rethinking data augmentation for image super-resolution: A comprehensive analysis and a new strategy. In *CVPR*, 2020. 4, 8
- [54] Y. Yuan, X. Zheng, and X. Lu. Hyperspectral image super-resolution by transfer learning. *IEEE Journal of Selected Topics in Applied Earth Observations and Remote Sensing*, 10(5):1963–1974, 2017. 2
- [55] R. H. Yuhas, A. F. Goetz, and booktitle=JPL, Summaries of the Third Annual JPL Airborne Geoscience Workshop year = 1992 J. W. Boardman, title=Discrimination among semi-arid landscape endmembers using the spectral angle mapper (sam) algorithm. 6
- [56] Amir Zamir, Alexander Sax, Teresa Yeo, Oğuzhan Kar, Nikhil Cheerla, Rohan Suri, Zhangjie Cao, Jitendra Malik, and Leonidas Guibas. Robust learning through cross-task consistency. In *CVPR*. 2020. 2
- [57] Hongyi Zhang, Moustapha Cisse, Yann N. Dauphin, and David Lopez-Paz. mixup: Beyond empirical risk minimization. In *International Conference on Learning Representations*, 2018. 2, 4, 8
- [58] Lei Zhang, Jiangtao Nie, Wei Wei, Yanning Zhang, Shengcai Liao, and Ling Shao. Unsupervised adaptation learning for hyperspectral imagery super-resolution. In *CVPR*, 2020. 2
- [59] Yulun Zhang, Yapeng Tian, Yu Kong, Bineng Zhong, and Yun Fu. Residual dense network for image super-resolution. 2

- [60] Y. Zhao, Jinxiang Yang, Qingyong Zhang, L. Song, Y. Cheng, and Q. Pan. Hyperspectral imagery super-resolution by sparse representation and spectral regularization. *EURASIP Journal on Advances in Signal Processing*, 2011:1–10, 2011. 2
- [61] Y. Zhou, A. Rangarajan, and P. D. Gader. An integrated approach to registration and fusion of hyperspectral and multi-spectral images. *IEEE Transactions on Geoscience and Remote Sensing*, 58(5):3020–3033, 2020. 2
- [62] Zhou Wang, A. C. Bovik, H. R. Sheikh, and E. P. Simoncelli. Image quality assessment: from error visibility to structural similarity. *IEEE Transactions on Image Processing*, 13(4):600–612, 2004. 6

Supplementary Material

In this supplementary material, we provide

- results for scaling factor $\times 4$ under all the six metrics,
- results for scaling factor $\times 8$,
- more visual results.

Further results for scaling factor $\times 4$

Due to space limitation, only results under three metrics, *i.e.*, RMSE, MPSNR, and ERGAS, are reported in the main paper. Here, we report the results under all six considered metrics, *i.e.*, RMSE, CC, MPSNR, MSSIM, ERGAS, and SAM. For the case of scaling factor $\times 4$ and in the semi-supervised setting, the results on the CAVE dataset, the Harvard dataset, the NTIRE2020 dataset are shown in Table 6, Table 7 and Table 8, respectively. The results under the full-supervision setting on the CAVE dataset and on the Harvard dataset are reported in Table 9 and Table 10¹.

These tables show that our method outperforms other comparison methods by a large margin under all six metrics. All our three contributions are useful and their combination yields the best results. The conclusions we have in the main paper hold for all the six metrics.

Results for scaling factor $\times 8$

We also provide results for scaling factor $\times 8$. The results on the CAVE, the Harvard, and the NTIRE2020 datasets in the semi-supervised setting are shown in Table 11, Table 12, and Table 13, respectively. It is evident from these tables that our method also outperforms other methods significantly and consistently for scaling factor $\times 8$. The same trend is observed for both $\times 4$ and $\times 8$ that all our three contributions are useful and their combination yields the best results. This demonstrates the applicability of our method across different scaling factors.

¹The results on the NTIRE2020 dataset have not completed before the deadline unfortunately, but the obtained results show that the variants of our method with only a subset of our contributions already outperform all the competing methods.

More visual results

We also provide more visual results on the NTIRE2020 datasets. For visualization, we use the same method as in the main paper. More specifically, we sample the 5th band, the 15th band and the 25th band of the hyperspectral image and assemble them together as an RGB image for visualization. The results of all methods on two different images for scaling factor $\times 8$ are provided in Fig. 4 and Fig. 5. To facilitate the comparison, we also show the error maps of all methods. The values in the error maps are the L2 distance between the predicted pixel values and the ground-truth pixel values, averaged over the three bands. It is clear from the visual results that our method generates better results than other methods. For instance, it produces sharper boundaries and less artefact.

Methods	Components			Metrics					
	RGB_SR	<i>Spec Mixup</i>	SSL	RMSE ↓	CC ↑	MPSNR ↑	MSSIM ↑	ERGAS ↓	SAM ↓
Ours				0.01282	0.99255	41.38106	0.96382	3.99731	6.17381
Ours	✓			0.01191	0.99343	42.01763	0.96661	3.63288	4.87344
Ours		✓		0.01246	0.99321	42.08879	0.96508	3.54516	3.78728
Ours	✓	✓		0.01173	0.99364	42.57401	0.96717	3.40209	3.59636
Ours	✓		✓	0.01187	0.99342	42.21247	0.96674	3.53264	4.46704
Ours (final)	✓	✓	✓	0.01138	0.99389	42.74453	0.96806	3.31609	3.57381
BicubicInt.	-	-	-	0.01856	0.98682	38.73800	0.94197	5.27190	4.17591
GDRRN [35]	-	-	-	0.02048	0.98479	37.59559	0.92286	5.76242	7.77988
3DFCNN [38]	-	-	-	0.01686	0.97777	38.32237	0.94694	8.81439	8.59455
SSPSR [26]	-	-	-	0.01349	0.99115	41.46318	0.96104	3.91284	4.07686
MCNet [34]	-	-	-	0.01362	0.98964	41.28549	0.96029	4.16636	4.65331

Table 6: Results of our method and other comparison methods on the CAVE dataset in the semi-supervised setting for the $\times 4$ case.

Methods	Components			Metrics					
	RGB_SR	<i>Spec Mixup</i>	SSL	RMSE ↓	CC ↑	MPSNR ↑	MSSIM ↑	ERGAS ↓	SAM ↓
Ours				0.01411	0.95826	40.42362	0.92569	3.20297	2.58523
Ours	✓			0.01366	0.95959	40.69577	0.92768	3.11316	2.56292
Ours		✓		0.01375	0.95951	40.63699	0.92726	3.12395	2.54555
Ours	✓	✓		0.01348	0.96020	40.80286	0.92853	3.07281	2.54400
Ours	✓		✓	0.01351	0.96013	40.81661	0.92864	3.06886	2.55412
Ours (final)	✓	✓	✓	0.01335	0.96049	40.89392	0.92907	3.03947	2.53253
BicubicInt.	-	-	-	0.01678	0.94994	38.89758	0.90925	3.80698	2.61754
GDRRN [35]	-	-	-	0.01655	0.93686	38.24997	0.90996	4.72408	3.26193
3DFCNN [38]	-	-	-	0.01578	0.95095	39.30286	0.91648	3.66444	2.72254
SSPSR [26]	-	-	-	0.01422	0.95789	40.34668	0.92474	3.22915	2.59564
MCNet [34]	-	-	-	0.01463	0.95749	40.18194	0.92286	3.27906	2.64800

Table 7: Results of our method and other comparison methods on the Harvard dataset in the semi-supervised setting for the $\times 4$ case.

Methods	Components			Metrics					
	RGB_SR	<i>Spec Mixup</i>	SSL	RMSE ↓	CC ↑	MPSNR ↑	MSSIM ↑	ERGAS ↓	SAM ↓
Ours				0.01675	0.99049	37.76302	0.93697	2.36922	1.35066
Ours	✓			0.01583	0.99135	38.21667	0.94195	2.27241	1.48222
Ours		✓		0.01542	0.99182	38.56435	0.94279	2.16249	1.29018
Ours	✓	✓		0.01515	0.99198	38.75436	0.94310	2.11092	1.23994
Ours	✓		✓	0.01547	0.99186	38.55183	0.94279	2.16476	1.29852
Ours (final)	✓	✓	✓	0.01507	0.99206	38.83877	0.94335	2.09341	1.22883
BicubicInt.	-	-	-	0.02353	0.98297	34.74012	0.90050	3.19014	3.89655
GDRRN [35]	-	-	-	0.02484	0.97852	33.94214	0.89828	3.68688	3.54982
3DFCNN [38]	-	-	-	0.02080	0.98629	35.83412	0.91539	2.82781	1.66409
SSPSR [26]	-	-	-	0.01721	0.98991	37.58708	0.93317	2.37159	1.53442
MCNet [34]	-	-	-	0.01613	0.99111	38.45578	0.93931	2.19636	1.45320

Table 8: Results of our method and other comparison methods on the NTIRE2020 dataset in the semi-supervised setting for the $\times 4$ case.

Methods	Components		Metrics					
	RGB_SR	<i>Spec Mixup</i>	RMSE ↓	CC ↑	MPSNR ↑	MSSIM ↑	ERGAS ↓	SAM ↓
Ours			0.01196	0.99350	42.38359	0.96631	3.45903	4.00592
Ours	✓		0.01109	0.99422	42.73668	0.96869	3.35884	4.17068
Ours		✓	0.01134	0.99397	42.88402	0.96798	3.28051	3.47102
Ours (final)	✓	✓	0.01068	0.99447	43.32421	0.96980	3.11799	3.68885
GDRRN [35]	-	-	0.01629	0.98975	39.74705	0.94418	4.52683	5.39660
3DFCNN [38]	-	-	0.01583	0.98538	39.21786	0.95165	5.41798	6.49516
SSPSR [26]	-	-	0.01245	0.99317	42.13787	0.96457	3.55146	3.83398
MCNet [34]	-	-	0.01245	0.99283	42.25978	0.96465	3.56246	3.84976

Table 9: Results of our method and other comparison methods on the CAVE dataset in the fully supervised case for **the $\times 4$ case**.

Methods	Components		Metrics					
	RGB_SR	<i>Spec Mixup</i>	RMSE ↓	CC ↑	MPSNR ↑	MSSIM ↑	ERGAS ↓	SAM ↓
Ours			0.01344	0.96101	40.91014	0.92836	3.01039	2.50704
Ours	✓		0.01325	0.96165	41.03709	0.92949	2.96643	2.49562
Ours		✓	0.01317	0.96200	41.08568	0.93056	2.95718	2.49771
Ours (final)	✓	✓	0.01321	0.96178	41.05925	0.93016	2.96496	2.49897
GDRRN [35]	-	-	0.01484	0.95102	39.62759	0.92013	3.67932	2.78624
3DFCNN [38]	-	-	0.01519	0.95411	39.66271	0.91944	3.47738	2.63534
SSPSR [26]	-	-	0.01352	0.96059	40.81499	0.92806	3.05007	2.51185
MCNet [34]	-	-	0.01405	0.96009	40.59229	0.92658	3.10529	2.59147

Table 10: Results of our method and other comparison methods on the Harvard dataset in the fully supervised case for **the $\times 4$ case**.

Methods	Components			Metrics					
	RGB_SR	<i>Spec Mixup</i>	SSL	RMSE ↓	CC ↑	MPSNR ↑	MSSIM ↑	ERGAS ↓	SAM ↓
Ours				0.02459	0.97233	35.89888	0.90591	7.11644	7.50539
Ours	✓			0.02300	0.97545	36.50494	0.91358	6.62181	6.89221
Ours		✓		0.02339	0.97705	36.64775	0.91078	6.45075	6.40468
Ours	✓	✓		0.02209	0.97923	37.14066	0.91748	6.14668	6.24141
Ours	✓		✓	0.02237	0.97732	36.87625	0.91685	6.34934	6.31945
Ours (final)	✓	✓	✓	0.02154	0.97963	37.35599	0.92070	6.00466	5.62054
BicubicInt.	-	-	-	0.03042	0.96665	34.22211	0.87386	8.43509	5.89620
GDRRN [35]	-	-	-	0.03473	0.95693	32.93635	0.83473	9.85545	11.05589
3DFCNN [38]	-	-	-	0.02920	0.90523	32.90242	0.87942	16.72651	10.43919
SSPSR [26]	-	-	-	0.02485	0.97260	35.88966	0.89926	7.03941	7.33639
MCNet [34]	-	-	-	0.02802	0.95804	34.31165	0.88028	10.29851	7.68969

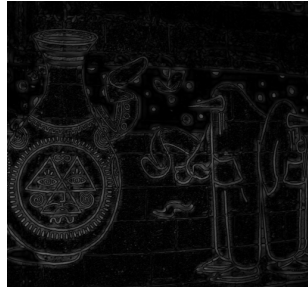
Table 11: Results of our method and other comparison methods on the CAVE dataset in the semi-supervised setting for **the $\times 8$ case**.



(a) Ground Truth



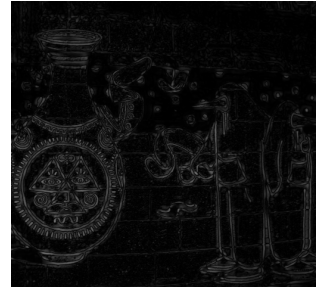
(b) Bicubic Interpolation



(c) Error of Bicubic



(d) GDRRN [35]



(e) Error of GDRRN



(f) 3DFCNN [38]



(g) Error of 3DFCNN



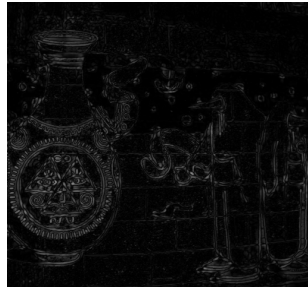
(h) SSPSR [26]



(i) Error of SSPSR



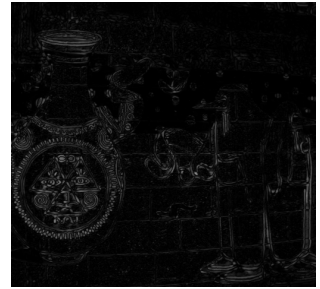
(j) MCNet [34]



(k) Error of MCNet



(l) Ours



(m) Error of Ours

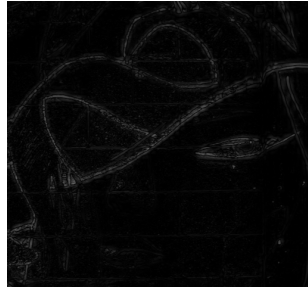
Figure 4: Exemplar results of $\times 8$ by our method and all comparison methods. The error is L2 distance to the ground-truth pixel values, averaged over the three bands.



(a) Ground Truth



(b) Bicubic Interpolation



(c) Error of Bicubic



(d) GDRRN [35]



(e) Error of GDRRN



(f) 3DFCNN [38]



(g) Error of 3DFCNN



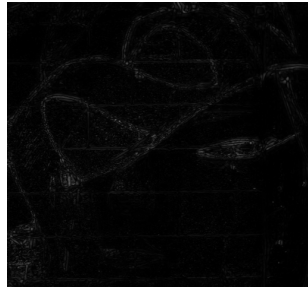
(h) SSPSR [26]



(i) Error of SSPSR



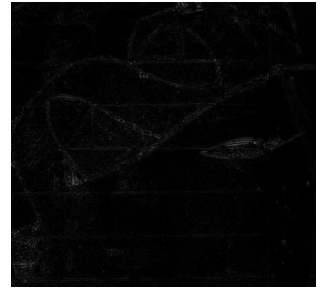
(j) MCNet [34]



(k) Error of MCNet



(l) Ours



(m) Error of Ours

Figure 5: Exemplar results of $\times 8$ by our method and all comparison methods. The error is L2 distance to the ground-truth pixel values, averaged over the three bands.

Methods	Components			Metrics					
	RGB_SR	<i>Spec Mixup</i>	SSL	RMSE ↓	CC ↑	MPSNR ↑	MSSIM ↑	ERGAS ↓	SAM ↓
Ours				0.02263	0.92668	36.65405	0.86476	4.85976	2.91037
Ours	✓			0.02127	0.93172	37.14154	0.87229	4.58089	2.88299
Ours		✓		0.02219	0.92789	36.85938	0.86725	4.76278	2.89283
Ours	✓	✓		0.02117	0.93241	37.18768	0.87294	4.55818	2.85549
Ours	✓		✓	0.02116	0.93218	37.21642	0.87269	4.55045	2.88124
Ours (final)	✓	✓	✓	0.02100	0.93450	37.35231	0.87345	4.54990	2.88230
BicubicInt.	-	-	-	0.02495	0.91446	35.74092	0.84966	5.47721	3.00931
GDRRN [35]	-	-	-	0.02389	0.91131	35.64417	0.85316	5.72871	3.41440
3DFCNN [38]	-	-	-	0.02379	0.91813	36.05515	0.85651	5.21924	3.09288
SSPSR [26]	-	-	-	0.02282	0.92266	36.45639	0.86174	4.99781	3.07039
MCNet [34]	-	-	-	0.02348	0.92343	36.39212	0.85940	5.05722	3.14259

Table 12: Results of our method and other comparison methods on the Harvard dataset in the semi-supervised setting for **the $\times 8$ case**.

Methods	Components			Metrics					
	RGB_SR	<i>Spec Mixup</i>	SSL	RMSE ↓	CC ↑	MPSNR ↑	MSSIM ↑	ERGAS ↓	SAM ↓
Ours				0.02969	0.97146	32.83078	0.84733	4.04429	1.88851
Ours	✓			0.02839	0.97343	33.23283	0.85401	3.89444	1.83394
Ours		✓		0.03004	0.97055	32.75617	0.84575	4.08821	1.90378
Ours	✓		✓	0.02800	0.97355	33.23400	0.85870	3.88999	1.83009
Ours	✓	✓		0.02809	0.97385	33.33009	0.85599	3.85485	1.79814
Ours (final)	✓	✓	✓	0.02799	0.97560	33.45620	0.86001	3.84456	1.76943
BicubicInt.	-	-	-	0.03961	0.95195	29.95891	0.78926	5.45947	5.24567
GDRRN [35]	-	-	-	0.03596	0.95545	30.67236	0.80217	5.12654	3.21549
3DFCNN [38]	-	-	-	0.38575	-0.57977	9.17534	-0.47680	61.62476	163.56878
SSPSR [26]	-	-	-	0.03268	0.96529	31.78969	0.82646	4.49521	2.25976
MCNet [34]	-	-	-	0.03276	0.96623	31.96291	0.82932	4.41695	2.38619

Table 13: Results of our method and other comparison methods on the NTIRE2020 dataset in the semi-supervised setting for **the $\times 8$ case**.